Ultrasonics 89 (2018) 74–83

Contents lists available at ScienceDirect

Ultrasonics

journal homepage: www.elsevier.com/locate/ultras

Non-contact ultrasonic gas flow metering using air-coupled leaky Lamb waves

Zichuan Fan[b,d], Wentao Jiang[a,c], William M.D. Wright[a,*]

[a] Department of Electrical and Electronic Engineering, University College Cork (UCC), Cork, Ireland
[b] School of Computer and Information Science, Southwest University, Chongqing 400715, People's Republic of China
[c] Department of Cardiovascular Sciences, Katholieke Universiteit Leuven (KU Leuven), 3000 Leuven, Belgium
[d] School of Automation Science and Electrical Engineering, Beihang University, Beijing 100191, People's Republic of China

ARTICLE INFO

Keywords:
Non-contact flow metering
Air-coupled leaky Lamb waves
Airborne ultrasound
COMSOL Multiphysics® modelling
Ultrasonic wave visualization

ABSTRACT

This paper describes a completely non-contact ultrasonic method of gas flow metering using air-coupled leaky Lamb waves. To show proof of principle, a simplified representation of gas flow in a duct, comprising two separated thin isotropic plates with a gas flowing between them, has been modelled and investigated experimentally. An airborne compression wave emitted from an air-coupled capacitive ultrasonic transducer excited a leaky Lamb wave in the first plate in a non-contact manner. The leakage of this Lamb wave crossed the gas flow at an angle between the two plates as a compression wave, and excited a leaky Lamb wave in the second plate. An air-coupled capacitive ultrasonic transducer on the opposite side of this second plate then detected the airborne compression wave leakage from the second Lamb wave. As the gas flow shifted the wave field between the two plates, the point of Lamb wave excitation in the second plate was displaced in proportion to the gas flow rate. Two such measurements, in opposite directions, formed a completely non-contact contra-propagating Lamb wave flow meter, allowing measurement of the flow velocity between the plates. A COMSOL Multiphysics® model was used to visualize the wave fields, and accurately predicted the time differences that were then measured experimentally. Experiments using different Lamb wave frequencies and plate materials were also similarly verified. This entirely non-contact airborne approach to Lamb wave flow metering could be applied in place of clamp-on techniques in thin-walled ducts or pipes.

1. Introduction

Gas flow measurement is an important part of industrial instrumentation, encompassing a wide range of applications from natural gas distribution, compressed air systems, air conditioning, and process control [1]. A clamp-on ultrasonic flow meter does not obstruct the pipe, nor is it in direct contact with the fluid, which eliminates any pressure loss. It may also be installed without any mechanical modification of the pipe or duct, or interruption to the flow or process [2,3]. To obtain accurate ultrasonic measurements, an appropriate method of contact or coupling is required to facilitate the transmission of ultrasound between the transducer and the pipe wall. Different methods may be chosen according to the process temperature and whether long-term or short-term use is required [4]. Variation in the couplant reliability and temperature compatibility may adversely affect the operation of a clamp-on ultrasonic flow meter.

Airborne or air-coupled ultrasound could provide a non-contact couplant-free approach for flow measurement. As an alternative for immersion or contact testing technologies, non-contact air-coupled ultrasonic testing and non-destructive evaluation (NDE) has been used in an increasing number of industrial applications in recent years, due to the improvements in transducer efficiency, electronics and signal processing [5,6]. For airborne ultrasound, the large specific acoustic impedance mismatch that exists between air and most solids is still one of the largest obstacles to a non-contact couplant-free approach for clamp-on or external flow measurement methods. Previous work [7] has implemented liquid flow measurement in a pipe using highly focussed air-coupled ultrasonic beams and bulk waves, but air-coupled non-contact gas flow measurement is particularly difficult due to the additional mismatch in specific acoustic impedance between the pipe and the flowing gas.

Lamb waves and other guided waves are often used in air-coupled ultrasonic testing, particularly in plate-like structures that are thin in comparison to the wavelength [8,9]. Not only can Lamb waves propagate over long distances, but they also continuously leak energy into the adjacent air or other fluid as they travel. Lamb waves are commonly

* Corresponding author.
E-mail address: bill.wright@ucc.ie (W.M.D. Wright).

https://doi.org/10.1016/j.ultras.2018.04.008
Received 21 December 2017; Received in revised form 20 April 2018; Accepted 22 April 2018
Available online 23 April 2018
0041-624X/

used in clamp-on ultrasonic flow meters, as significant energy can be transferred into the fluid under test, but direct contact coupling is usually still required [1–3,10] or miniature sensors may be placed directly in the flow [11,12].

Therefore, it should be feasible to accomplish entirely non-contact ultrasonic gas flow measurement using air-coupled leaky Lamb waves instead of a clamp-on flow meter. In this paper, we have investigated a prototype system used with a simplified representation of a duct, comprising two thin plates separated by a gap with air as the gaseous fluid flowing between them, to show proof of principle. This was a two-dimensional approximation of a square duct or pipe, where only axial Lamb waves were considered, and transverse or circumferential Lamb waves were neglected: hence, the equivalent pipe diameter was assumed to be large compared to the duct or pipe wall thickness, and the ultrasonic wavelength. It was not a study of the propagation of Lamb waves in pipe walls, which has already been investigated by many authors, both analytically and numerically [13–15]. Additionally, the model to investigate this non-contact flow measurement, which is highly dependent on flow velocity, could be demonstrated without adding any three-dimensional complexity as it was not specific to parameters like fluid pressure and pipe size.

In the work described here, a bulk compression wave was generated in the ambient air, and entered the first plate to excite a Lamb wave in a non-contact manner. Leakage of this first propagating Lamb wave passed through the flowing gaseous fluid between the plates as a bulk compression wave, and then entered the second plate to generate a second Lamb wave. Leakage from this second propagating Lamb wave into the ambient air was then detected by a non-contact airborne receiver. As the leaky wave (the bulk compression wave) travelling between the two plates was shifted by the gaseous fluid flow, the excitation position of the second Lamb wave was displaced proportionally to the velocity of the flow. Thus, the flow velocity could be obtained by detecting the time difference between contrapropagating signals, as per a classical clamp-on Lamb wave flow meter [10].

In Section 2 of this paper, an analytical model and a corresponding COMSOL Multiphysics® simulation of the implemented non-contact flow measurement system are described. Section 3 covers the results and analysis of the model and simulations, where of the excitation point of the second Lamb wave by the gas flow is shown and verified. Experimental measurements are describe in Section 4, and compared with the simulations and discussed in Section 5. Additional experiments with differences in receiving distance, ultrasonic frequency, plate thickness and plate material are presented and discussed. Conclusions about the non-contact method are then drawn in Section 6.

2. Modelling and simulation

The aim of this study was to focus on the feasibility of non-contact ultrasonic gas flow measurement based on air-coupled leaky Lamb waves, so it was not intended to be specific to parameters such as the type of ultrasonic transducers used, gas pressure, pipe size, and fluid type, as they are not directly relevant to the feasibility and also would have added significant computational complexity to the model. A simplified two-dimensional representation of gas flow in a square or rectangular duct, comprising two thin plates separated by a gap, with air as the gaseous fluid flowing between them as shown in Fig. 1, was investigated. This model provided a clear relationship between the flow velocity, non-contact Lamb waves and time delay.

2.1. The general analytical model – zero flow

The general analytical model may be described as follows. As shown in Fig. 1, the centre normal of the transmitter (Tx) is inclined at an angle α_{Tx} to the surface normal of Plate 1, at a distance of r_{Tx}. Hence, the time t_{Tx} for an airborne ultrasonic compression wave to travel across this air path is:

$$t_{Tx} = \frac{r_{Tx}}{c_a} \tag{1}$$

where c_a is the speed of sound in the ambient air. This time will also include any delay due to the transduction process and the electronics. The first Lamb wave is then assumed to be generated instantaneously in Plate 1 at the point of entry x_{in} after time t_{Tx}, and propagate along Plate 1, leaking into the flowing air between the two plates as another compression wave. At an angle β_0, according to Snell's Law, and at zero flow ($v_f = 0$ m/s), this compression wave will cross the gap between the two plates along a path L_0 in a time t_L, given by:

$$t_L = \frac{L_0}{c_f} = \frac{D}{c_f \cos\beta_0}, \tag{2}$$

where c_f is the speed of sound in the fluid between the plates and D is the plate separation. The compression wave will then enter Plate 2 at a point displaced horizontally from the entry point x_{in} in Plate 1 by a distance $x_0 = D \tan \beta_0$, and generate a second Lamb wave, which will then propagate along Plate 2 with group velocity c_g and leak into the ambient air between Plate 2 and the receiver (Rx) as another airborne ultrasonic compression wave. To optimise the reception of the leaky waves at the exit point x_{out} from Plate 2, the centre normal of the receiver (Rx) will be inclined at an angle α_{Rx} to the surface normal of Plate 2, at a distance of r_{Rx}, which means that the Lamb waves in Plate 2 propagate a distance d_0 in the plate, given by:

$$d_0 = x_P - x_0 = x_P - D\tan\beta_0, \tag{3}$$

where $x_P = x_{out} - x_{in}$, with a corresponding propagation time t_{d0} of:

$$t_{d0} = \frac{d_0}{c_g} = \frac{x_P - D\tan\beta_0}{c_g}. \tag{4}$$

Finally, the time t_{Rx} for the ultrasound to travel across the air path r_{Rx} between Plate 2 and the receiver (Rx) is given by:

$$t_{Rx} = \frac{r_{Rx}}{c_a}, \tag{5}$$

which also includes any delay due to the transduction process and receiver electronics, giving a total propagation time t_0 between Tx and Rx at zero flow of:

$$t_0 = t_{Tx} + t_L + t_{d0} + t_{Rx} = \frac{r_{Tx}}{c_a} + \frac{D}{c_f \cos\beta_0} + \frac{x_P - D\tan\beta_0}{c_g} + \frac{r_{Rx}}{c_a}. \tag{6}$$

2.2. The general analytical model – non-zero flow

When $v_f \neq 0$, the leaky waves crossing the gap between the two plates will be displaced either towards Tx or towards Rx along a new equivalent path L_f, depending on the direction of the flow. However, the time taken for the leaky waves to cross the gap between the two plates will still be t_L, as the angle that the Lamb waves in Plate 1 leak into the flow will still be β_0 and the velocity vector normal to the surface of Plate 1 will be identical, irrespective of the magnitude of the flow v_f. Hence, in the time t_L that it takes the leaky waves to cross the gap between the two plates, the waves will have been displaced horizontally by the flow by a distance x_f, given by:

$$x_f = \pm v_f t_L = \pm \frac{v_f D}{c_f \cos\beta_0}, \tag{7}$$

which then increases or decreases the distance d_f that the Lamb waves propagate in Plate 2 to:

$$d_f = x_P - x_0 - x_f = x_P - D\left(\tan\beta_0 \pm \frac{v_f}{c_f}\sec\beta_0\right), \tag{8}$$

with a corresponding Lamb wave propagation time t_{df} in Plate 2 of:

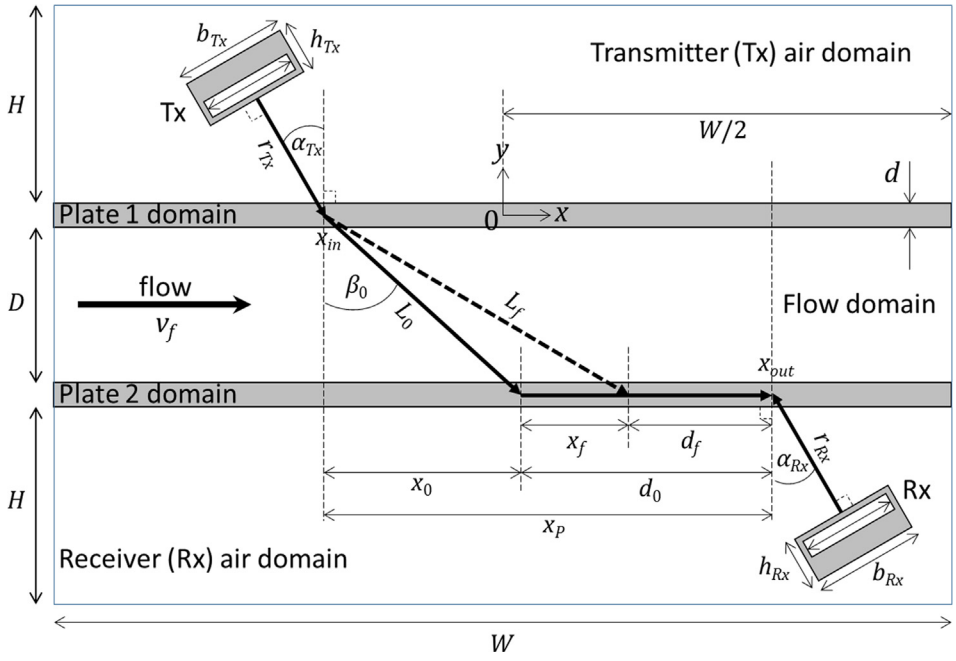

Fig. 1. Schematic diagram of the non-contact ultrasonic flow measurement geometry.

$$t_{df} = \frac{d_f}{c_g} = \frac{x_P - D\left(\tan\beta_0 \pm \frac{v_f}{c_f}\sec\beta_0\right)}{c_g}. \tag{9}$$

This then gives a total propagation time t_f between Tx and Rx at a flow v_f of:

$$t_f = t_{Tx} + t_L + t_{df} + t_{Rx} = \frac{r_{Tx}}{c_a} + \frac{D}{c_f\cos\beta_0} + \frac{x_P - D\left(\tan\beta_0 \pm \frac{v_f}{c_f}\sec\beta_0\right)}{c_g} + \frac{r_{Rx}}{c_a}. \tag{10}$$

If the geometrical parameters and fluid properties are known with sufficient accuracy, then the mean fluid flow velocity, v_f, may be calculated directly from (10). For identical plates, and identical transducer separations r_{Tx} and r_{Tx}, it is clear that the air gap times t_{Tx} and t_{Rx} will be the same, and if the roles of the transmitter Tx and the receiver Rx are reversed, t_L will still be the same and only t_{df} will be affected by the flow. Hence, the difference in total propagation times Δt_f for contra-propagating Lamb waves, may also be used to determine the average fluid flow rate v_f thus:

$$\Delta t_f = \frac{2Dv_f}{c_g c_f \cos\beta_0}, \tag{11}$$

$$v_f = \frac{c_g c_f \cos\beta_0}{2D}\Delta t_f. \tag{12}$$

Hence, prior knowledge of just the plate separation, the sound speed in the fluid at rest, the Lamb wave velocities at the specified frequencies and Snell's Law, are required.

2.3. Lamb wave modes

Specific Lamb wave modes that propagate in plates of a certain material and thickness can be determined by selecting the correct frequency, according to the velocity dispersion from the Rayleigh-Lamb frequency equations [16]. The dispersion curves for the antisymmetric (A_n) and symmetric (S_n) modes in the isotropic plates are readily derived, as shown in Fig. 2 for polycarbonate. At frequency-thickness products of less than 0.5 MHz·mm, only the zero-order modes A_0 and S_0

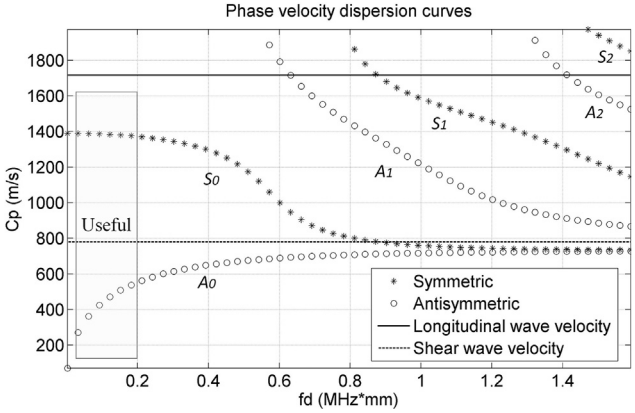

Fig. 2. Phase velocity dispersion curves of the first three symmetric and antisymmetric modes in polycarbonate.

exist. It can be seen that the A_0 mode disperses significantly with the frequency-thickness product, whereas the S_0 mode disperses very little. In our study, the A_0 mode at frequency-thickness products of less than 0.2 MHz·mm were useful, as these provided various phase velocities at frequencies practical for air-coupled measurements, depending on the plate thickness. Hence, according to Snell's Law, various refraction angles of leaky waves between the two plates would also be obtained. As demonstrated in earlier work by the authors [17], the generation and detection of specific Lamb wave modes requires careful orientation of the transducers to prevent undesirable reflections at the plate surface. However, no significant loss in amplitude was observed within a transducer misalignment of ± 5°.

2.4. COMSOL multiphysics® modelling

The leaky wave which propagates in the same direction as the air flow (i.e. downstream) is firstly considered in the COMSOL Multiphysics® model. A similar approach was used for the leaky wave travelling against the direction of air flow (upstream). The specific mode of ultrasonic transducer operation was not required in the model. Airborne compression waves were used to generate the Lamb waves in

our study in a non-contact manner, so the principle of operation of the ultrasonic transducers is not relevant. Capacitive ultrasonic transducers have been shown to exhibit plane piston-like behaviour [17,18] and thus a uniform distribution of the pressure wave across the face of the transducer in the model would be a valid assumption. Therefore, similar behaviour has been simulated in this study to model the generation and detection of planar airborne compression waves.

The plate material was chosen to be homogenous polycarbonate to simplify the Lamb wave propagation calculations and ensure a low impedance mismatch between the air and the plates to enhance experimental production and detection of the signals. However, the modelling approach used here is not specific to the transducers and the plate material described, and with suitable modification can be used for other transducer types, more complicated plate structures such as curved pipe geometry, or more complex materials, such as fibre-reinforced composites.

2.4.1. General model details

Modelling was based on a finite element method and was implemented using the following steps:

(i) a two-dimensional geometric representation of the problem was subdivided into the following domains, as shown in Fig. 1: the ambient air domain containing the transmitter; the ambient air domain containing the receiver; the two polycarbonate plates; the flow domain between the two plates; the two transducers.
(ii) The governing equations and boundary conditions were defined for each domain. The impedance boundary provided by the Acoustics Module in COMSOL Multiphysics® was used to minimize the model geometry and the computational burden. However, this module could not directly simulate acoustic waves propagating in a moving fluid. Hence, a moving mesh method was applied, and the interaction of the leaky waves and the air flow could then be simulated.
(iii) The velocity profile in the flow domain was obtained from a simple open-channel flow model by using the Fluid Module in COMSOL Multiphysics®; the velocity profile data was then used as an input to the leaky wave propagation model built into the Acoustics Module.
(iv) Triangular mesh elements of 0.5 mm in the air domains and 0.25 mm in the plate and transducer domains, optimized based on the wavelengths, and a time step size of 0.04 μs, were chosen before running the simulations using a direct segregated solver, as described in more detail in earlier work [17]. The COMSOL Multiphysics® simulations converged when the relative tolerance was 0.01 (the default value was 0.001).

2.4.2. Geometry and material parameters

The plate geometry and material parameters used in the simulations were as shown in Table 1 and Table 2, respectively. The transmitter (Tx) with an active diameter a_{Tx} and overall width b_{Tx} and height h_{Tx} was located with its face centre at an offset radius r_{Tx} from the bulk wave entry point x_{in} in Plate 1 and rotated by the transmitter incidence angle α_{Tx}. Similarly, the receiver was located at an offset radius r_{Rx} from the bulk wave exit point x_{out} in Plate 2 and rotated by the receiver incidence angle α_{Rx}. The bulk wave entry and exit points were taken as the intersection of the transducer centre normal with the plate centreline. The coordinate origin was located in the centre of Plate 1 as shown in Fig. 1. The air flow was initially flowing from left to right, as shown. The transducers were orientated at specific incidence angles to optimise specific Lamb wave modes [19,20], according to velocity dispersion and Snell's Law. Thus, both the transmitter and receiver with a centre frequency of f were adjusted to the optimum angle of 50°, so the strongest signals at 100 kHz could be obtained.

Table 1
Geometric parameters used in the model.

Geometric parameters	Value
Plate length, W	500 mm
Plate thickness, d	1 mm
Transmitter/receiver air domain height, H	60 mm
Plate separation (flow domain), D	90 mm
Transmitter diameter, a_{Tx}	38.4 mm
Transmitter offset radius, r_{Tx}	30 mm
Transmitter angle, α_{Tx}	50°
Receiver diameter, a_{Rx}	38.4 mm
Receiver offset radius, r_{Rx}	30 mm
Receiver angle, α_{Rx}	50°
Overall transducer width, b_{Tx} and b_{Rx}	40 mm
Overall transducer height, h_{Tx} and h_{Rx}	20 mm
Ultrasonic frequency, f	100 kHz
Lamb wave inlet-outlet separation, $x_P = x_{out} - x_{in}$	150 mm

Table 2
Material property parameters used in the model.

Polycarbonate material properties	Value
Young's modulus, E	2.0 GPa
Poisson's ratio, ν	0.37
Density, ρ	1200 kg/m^3
Aluminium material properties	**Value**
Young's modulus, E	70 GPa
Poisson's ratio, ν	0.37
Density, ρ	2700 kg/m^3
Air properties	**Value**
Speed of sound, c_a	343 m/s

2.4.3. Governing equations and boundary conditions

Previous studies have focused more on the guided waves in the plates rather than the bulk waves leaking into the flowing fluid. Mode conversion will also occur at the interface of the air and the plate, and this has been modelled previously [17]. To resolve this issue in the simulation, the pressure acoustics and solid mechanics interfaces were combined using the Acoustic-Structure Interaction Module of COMSOL Multiphysics®, so that the acoustic pressure variations in the fluid domain and the structural deformation in the solid domain were then connected [21]. The parameters of air were those determined at standard atmospheric conditions. The impedance boundary was used at the outermost boundaries of the whole model to reduce reflections. Wave behaviour in the air flow was controlled by a moving mesh. The meshes here were deformed by the velocities calculated by preliminary flow simulations, described earlier. Any deformation of the plates due to the air flow was not included in the study, as the influences of the air pressure were negligible and the plates were regarded as undeformed during the very short time period covered by the whole simulation. The emitted airborne ultrasonic compression wave was simulated by applying a time-dependent boundary load $F(t)$ to the transmitter surface. The applied load is shown in Fig. 3, which was a smooth windowed sinusoid of ten cycles in length with a centre frequency f of 100 kHz and maximum amplitude F_0, given by:

$$F(t) = F_0 \sin(2\pi f t) \cdot \left(\sin\left(\frac{2\pi f t}{20} \right) \right)^2, \quad [t < 10/f]. \tag{13}$$

The received signals were measured in the simulations by calculating the mean displacement normal to the receiver surface, which will be deformed by the leaky wave propagating in the air. The simulation signal sampling rate was 25 MHz with a total signal time of 1 ms.

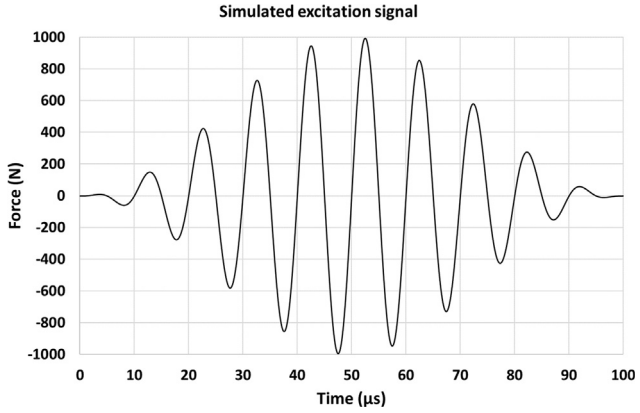

Fig. 3. Simulated windowed 10-cycle sinusoid excitation signal.

3. Simulation results and analysis

3.1. COMSOL multiphysics® simulation with no flow

It is important to accurately simulate the entire region where the leaky Lamb wave propagates, and to correctly visualize and interpret the results. Fig. 4 shows a sequence of snapshots of the wave fields in the plate and air domains obtained from the right sight part of the model, i.e. $0\,\text{mm} < x < 190\,\text{mm}$, at different times during the simulation with no flow between the plates. Note that the transmitter is not shown in these images, as its centre normal intersects Plate 1 at $x = -75\,\text{mm}$. The 1st and 3rd colour scales in each image Fig. 4 are von Mises equivalent stress, in N/m^2, in Plate 1 and Plate 2, respectively. The 2nd and 4th colour scales in each image in Fig. 4 are air pressure, in Pa, of leaky Lamb waves "LLW 1" in the flow region and "LLW 2" in the ambient air on the receiver side of Plate 2, respectively. As the same physical quantities span several orders of magnitude, the colour scales have different limits for better clarity.

Both symmetric and antisymmetric Lamb waves can occur. The symmetric S_0 mode has a much higher group velocity and had already propagated through the plate before these simulation times were visualized. Thus, it is clear in Fig. 4(a), that the pressure wave marked "1st Excited Wave", leaking energy into the air on both sides of Plate 1 between distances x of 100 mm and 190 mm, is the antisymmetric A_0 mode, as the leakage pattern of alternating high and low pressure wavefronts above the plate is matched by a respective pattern of low and high pressure wavefronts below the plate. This leaky wave from Plate 1 travels across the flow channel between the two plates as wave "LLW 1" at an angle, with the general direction of the wavefronts marked by an arrow. It reaches Plate 2 to excite a new Lamb wave marked "2nd Excited Wave" at a later time to, and displaced in x from, the initial Lamb wave in Plate 1. Consequently, a new leaky wave marked "LLW 2" is radiating energy into the ambient air beneath Plate 2 at a lower intensity, as shown in Fig. 4(b). The high intensity wavefronts above Plate 1 are the airborne compression waves reflected in the

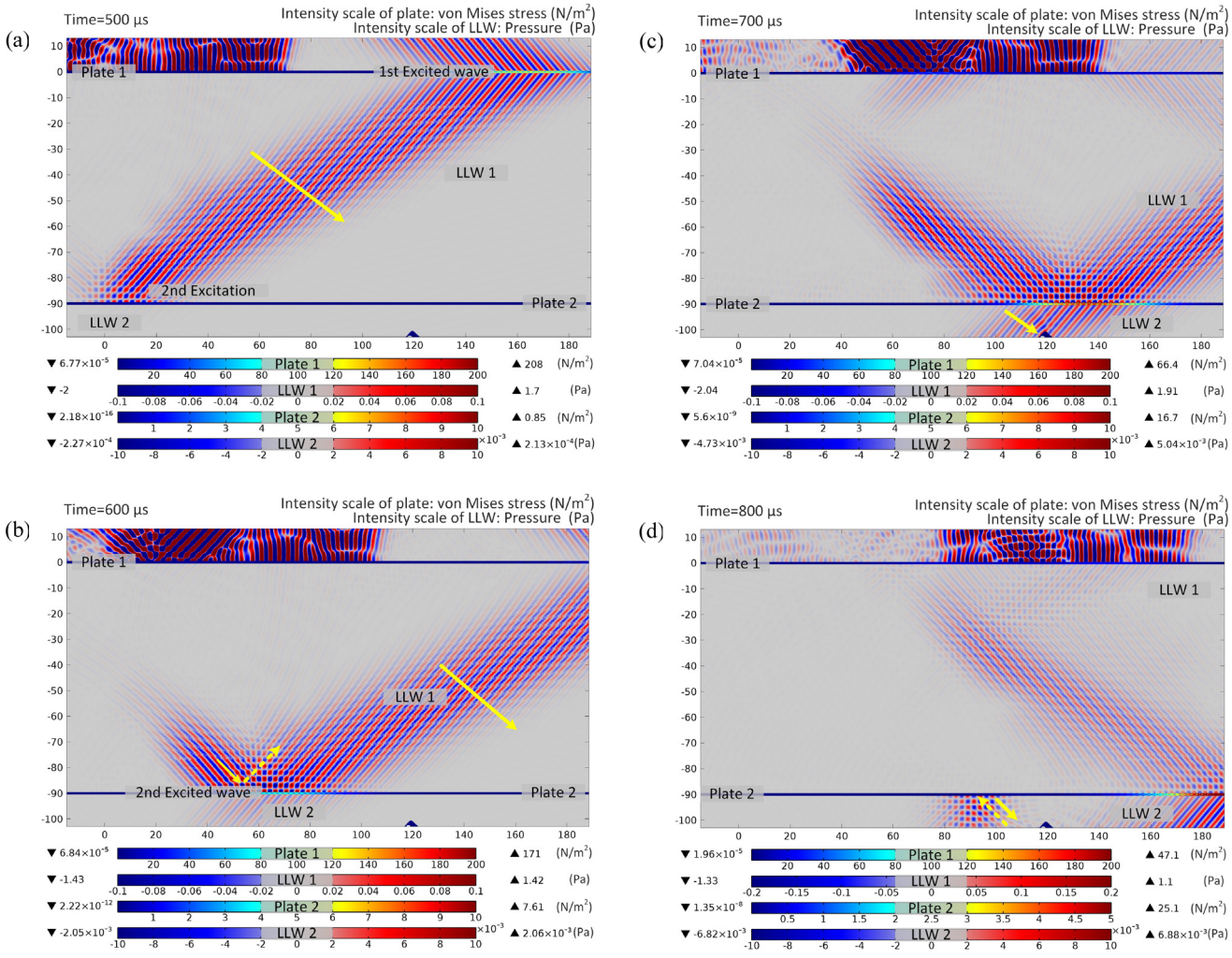

Fig. 4. Visualization of Lamb wave propagation in the plates and leakage into air at different simulation times of (a) 500 μs, (b) 600 μs, (c) 700 μs, and (d) 800 μs.

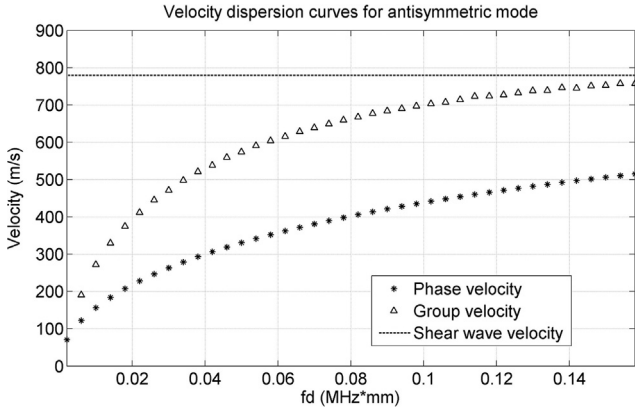

Fig. 5. Phase and group velocity dispersion curves for the A_0 mode at low frequency-thickness products.

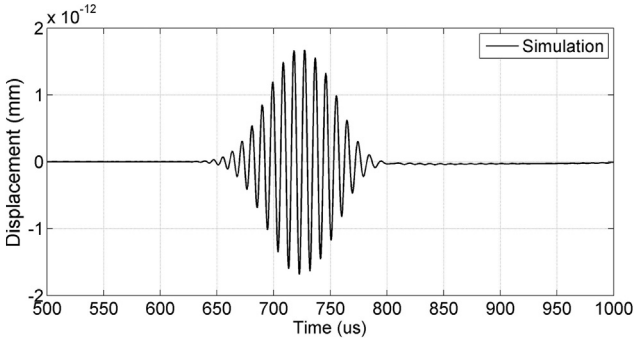

Fig. 6. Simulated signal obtained by the receiver.

air gap between the plate and the transmitter, and they travel at the sound speed in the ambient air.

In Fig. 4(b), it can also be seen that more leaky waves travel across the gap between the plates to reach Plate 2, and reflect at the surface of Plate 2 as indicated by the dashed arrow. The second Lamb wave generated in Plate 2 travels from left to right, and continuously leaks significant energy into the ambient air as wave "LLW 2" before being detected at the receiver (a corner of which is arrowed at $x = 120$ mm), as can be seen in Fig. 4(c), where wave "LLW 1" is also seen to be reflected by Plate 2 and propagate back towards Plate 1 at the same angle. In Fig. 4(d), bulk wave reflections in the air gap between Plate 2 and the receiver can be seen at a distance x between 80 mm and 100 mm, producing an interference pattern (arrowed).

3.2. Analytical model with no flow

The phase and group velocities at low frequency-thickness products may be calculated using the Rayleigh-Lamb frequency equations, and are illustrated in Fig. 5. It can be seen that a 100 kHz A_0 mode Lamb wave in a 1 mm thick polycarbonate plate (i.e., at 0.1 MHz·mm) travels with a group velocity of about 690 m/s and a phase velocity of 430 m/s, respectively. So the leaky wave at 100 kHz will propagate into the air from the plate at an angle of 52.9° for the A_0 mode, according to the refraction angle of the leaky wave determined by the phase velocities and Snell's Law.

The ultrasound travels a total distance of 209.2 mm in air at 343 m/s (i.e. $L_0 = 149.2$ mm between Plate 1 and Plate 2 at an angle of 52.9°, $r_{Tx} = 30$ mm between the transmitter and Plate 1, and $r_{Rx} = 30$ mm between Plate 2 and the receiver). The A_0 Lamb wave travels a distance $d_0 = 31$ mm in Plate 2 at the theoretical group velocity of 690 m/s, as shown in Fig. 5. Thus, the receiver will detect the signal at a time of 653.8 μs, by analytical calculation.

The corresponding signal from the simulation for the receiver for no flow is shown in Fig. 6. It is clear that an the signals starts between 650 μs and 660 μs, and reaches its maximum at about 710 μs, which is in good agreement with the values from the analytical calculations. Due to the large aperture (38.4 mm) and the angle of orientation of the transmitter and receiver, the left-hand edge of the transmitter and the right-hand edge of the receiver are closer to the plate than the right-hand edge of the transmitter and the left-hand edge of the receiver, respectively. This contributes to the additional temporal spreading of the received signal, as shown.

3.3. COMSOL multiphysics® simulation with air flow

Simulations with flowing air ($v_f > 0$) were then performed to calculate the expected time differences between the waves propagating upstream and downstream in the proposed non-contact contra-propagating Lamb wave flow meter. The propagation time difference is due to the displacement (Δx_{up} and Δx_{down}) of the Lamb wave excitation point, which is directly affected by the flow. For example, with the transmitter and receiver placed as shown in Fig. 1, the leaky wave between the two plates travels with the air flow (i.e., downstream), the excitation point is shifted right, and consequently, the Lamb wave propagation path and time in Plate 2 will decrease. Conversely, if the transmitter and receiver are reversed and the leaky wave between the two plates travels against the air flow (i.e., upstream), the excitation point is shifted left, and consequently, the Lamb wave propagation path and time in Plate 2 will increase.

To visualize how these displacements of the Lamb wave excitation point are affected by the air flow, a series of snapshots of the simulated wave fields is shown in Fig. 7 for an air flow velocity of 1.6 m/s between the two plates. The value of displacement was defined as the change in the propagation path from the excitation point of the Lamb wave in Plate 2 to the receiver.

In Fig. 7, the arrows indicate the position of the central maximum amplitude of the Lamb wave excited in Plate 2. Fig. 7(a) shows the position at zero flow, with a dashed line drawn at a fixed $x = 70$ mm for reference. In Fig. 7(b), it is clear that the central maximum has shifted left by -0.7 mm at an upstream flow rate of 1.6 m/s, with a dashed arrow showing the original position of this point at zero flow. Similarly, Fig. 7(c) shows the central maximum shifted right by $+0.7$ mm for a downstream flow of 1.6 m/s. When the transmitter and receiver positions are reversed in a contra-propagating flow meter configuration, identical shifts will occur in Plate 1.

3.4. Analytical model with air flow

According to Eq. (7) and using the relevant parameter values shown in Table 1, the excitation point of the Lamb wave in Plate 2 should have shifted by ± 0.702 mm, which is in excellent agreement with the COMSOL Multiphysics® simulations shown in Fig. 7. Thus, according to Eq. (11), the time shift of the received leaky Lamb waves should be ± 2.07 μs, depending on the flow direction. Simulated received signals, taken as the surface displacement of the centre of the receiver's surface in the model, are shown in Fig. 8 for different flow velocities for (a) downstream and (b) upstream directions, where there is a clear time shift proportional to the flow velocity, as expected. Fig. 9 shows a plot of these time differences against flow velocity from the simulation and a comparison with the values obtained from the analytical model, where it can be seen that, at a flow rate of 1.6 m/s, the time difference is 2.0 μs, which again is in excellent agreement.

4. Experimental measurements

The experimental set-up is shown in Fig. 10. The two plates used in the experiments were 500 mm × 250 mm in size, and were clamped vertically to prevent any axial deflection under their own weight.

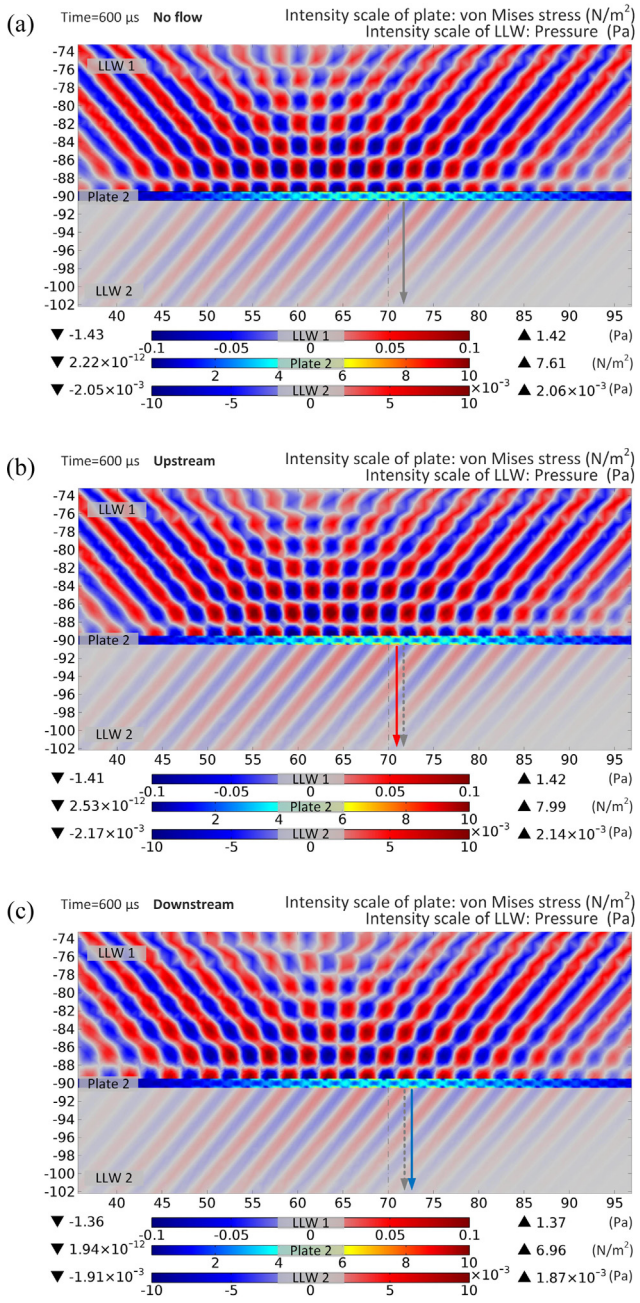

Fig. 7. Simulations of the shifted wave field and displacement of the Lamb wave excitation point (solid arrows) for (a) no flow, (b) upstream flow of 1.6 m/s giving a relative displacement of −0.7 mm, and (c) downstream flow of 1.6 m/s giving a relative displacement of +0.7 mm.

Polycarbonate plates of thickness 1 mm and 2 mm, and aluminium plates of thickness 1 mm were investigated in different experiments to validate the proposed technique. The ultrasonic transducers used were Senscomp 600 Series environmental grade transducers, with a nominal centre frequency of 50 kHz and a usable frequency range of up to 120 kHz.

An excitation signal of identical shape to the one used in the simulation shown previously in Fig. 3 was generated in MATLAB before being sent to a TTi TGA 1244 arbitrary waveform generator via a GPIB interface. It was then amplified to 300 V by a Falco WMA-300 high voltage amplifier, and combined with a bias voltage of +150 V generated by a Delta Electronika SM3004-D power supply before generating ultrasound at the transmitting Senscomp device. After propagation through the air gaps, plates and flow region, the ultrasonic

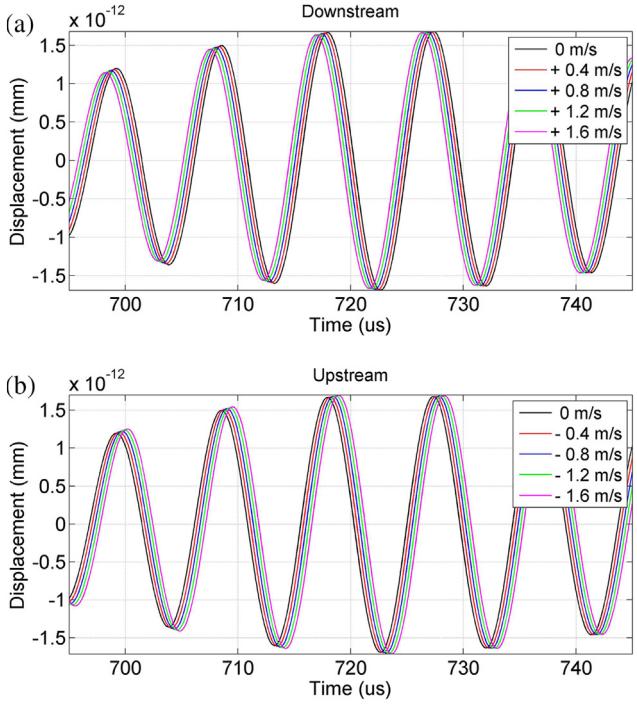

Fig. 8. Partial enlargement of simulated received signals (a) downstream, and (b) upstream.

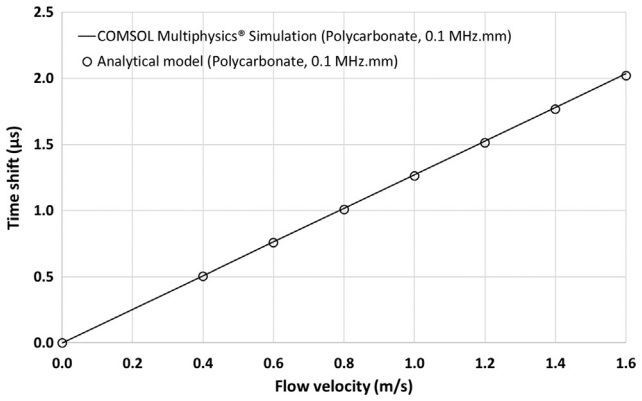

Fig. 9. Comparison of the time shift determined from by COMSOL simulation and analytical theory.

signals were detected by an identical Senscomp receiver connected to a Cooknell CA6/C charge amplifier powered by a Cooknell SU1/C power supply unit. The signal was then further amplified and band-pass filtered between 30 kHz and 300 kHz by an EG&G Model 5113 low-noise preamplifier. A Tektronix TDS 210 oscilloscope was then used to acquire the received signal for post processing and analysis in MATLAB via another GPIB interface. The signal-to-noise ratio (SNR) of the received signals was poor, with total attenuation on average −104.7 dB, so a rolling 128 signal average was used on the Tektronix oscilloscope in all experiments, to reduce random noise and minor rapid flow fluctuations.

The air flow between the two plates was generated by a small axial fan. To measure the velocity at any point in the flow region, a Lutron AM-4204 hot wire anemometer was used, with a flow measurement range from 0.2 m/s to 20 m/s and a resolution of 0.1 m/s. The velocity flow profile near the fan would not have been fully developed, thus the flow region between x_{in} and x_{out} used in the experiments was at a distance of 150 mm from the fan. The variation in velocity within this region was measured and found to be less than 0.2 m/s along a distance

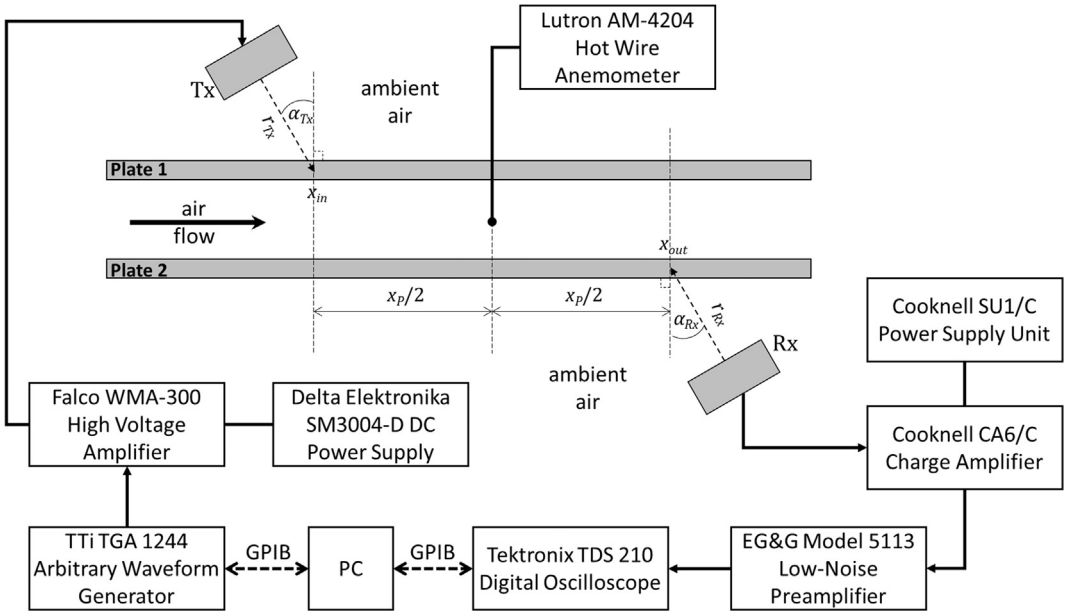

Fig. 10. Schematic diagram of experimental set-up.

of 100 mm in the x direction. So the average flow velocity considered in this work was the averaged value measured at the middle point of the flow channel, and it was increased from 0.4 m/s to 1.6 m/s in steps of 0.2 m/s. To emulate a contra-propagating flowmeter, the connections to the transmitter and receiver transducers were swapped over, reversing the direction of ultrasonic propagation in the system, and the measurements repeated.

Five experiments were performed, to show the feasibility of the proposed technique and to investigate the effects of using a different transducer separation x_P, different frequency Lamb waves, different thickness plates, and a different plate material, as follows:

(i) a configuration identical to that used in the COMSOL Multiphysics® simulations, using polycarbonate plates with a thickness d of 1 mm separated by a distance D of 90 mm, a frequency f of 100 kHz and a transducer separation x_P of 150 mm, as shown previously;
(ii) the same configuration as in (i), but with a different transducer separation distance x_P of 100 mm;
(iii) the same configuration as in (i), but at a different frequency f of 60 kHz, to vary the frequency-thickness product used;
(iv) the same configuration as in (i), but using a different thickness polycarbonate plate with $d = 2$ mm and frequency of $f = 50$ kHz, i.e. keeping the same frequency-thickness product of 0.1 MHz·mm;
(v) the same configuration as in (i), but using a different plate material of aluminium with $d = 1$ mm and $f = 40$ kHz.

5. Results and analysis

Typical experimental signals are shown in Fig. 11, obtained using polycarbonate plates 1 mm thick, an excitation signal frequency of 100 kHz, and with a horizontal transducer separation distance x_P of 150 mm, so that a direct comparison with the earlier COMSOL Multiphysics® models could be made. Fig. 11(a) shows a typical measured leaky A_0 Lamb wave, with the central region enlarged in (b) for the upstream and (c) for the downstream propagation directions. From Fig. 11(b) and (c), it can be seen the experimental signals are in excellent agreement with the simulations. It appears that the experimental time shift in Fig. 11(c) is slightly larger than that in Fig. 11(b) at the same velocity, because the transmitter was closer to the fan in the downstream configuration than the upstream configuration in the

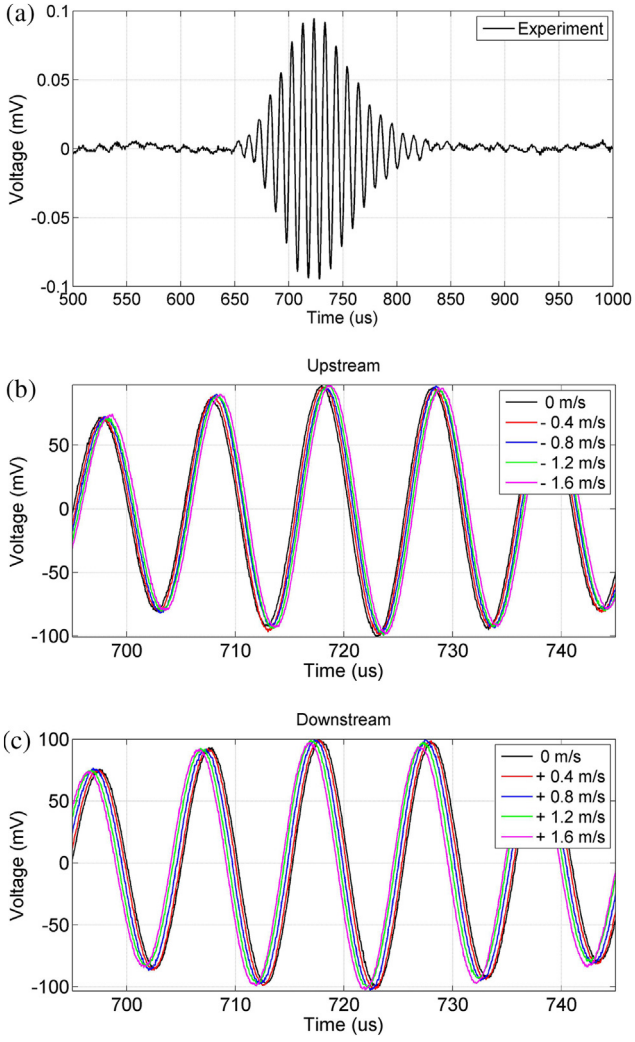

Fig. 11. Experimental signals collected by the receiver: (a) the leaky A_0 Lamb wave signal, (b) an enlargement of the shifted upstream signals, and (c) an enlargement of shifted downstream signals.

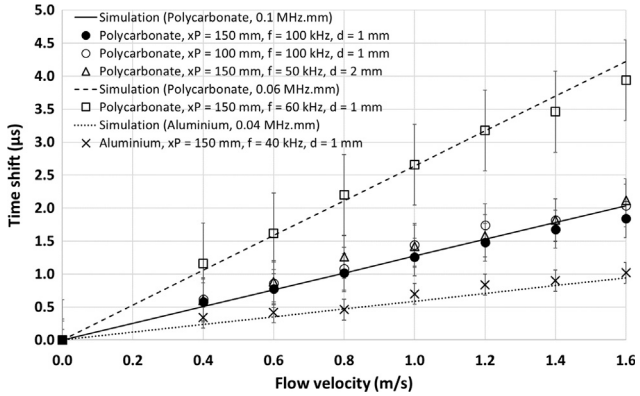

Fig. 12. A plot of time shift versus flow velocity for the same frequency-thickness products, different frequency-thickness products, different transducer separations, and different plate material. (Error bars are 1 standard deviation).

experiments. It should also be noted that as the upstream wave is shifted away from the receiver, the Lamb wave path and propagation time in the plate is increased, shifting the signals to the right in Fig. 11(b) as the flow rate increases. Conversely, the downstream wave is shifted to the left in Fig. 11(c), as expected.

Fig. 12 shows a comparison of the simulated and experimental time shifts obtained using a different transducer separation x_P, different frequency Lamb waves, different thickness plates, and a different plate material. According to Eq. (11), the time shift should be independent of the horizontal distance x_P between the transmitter and receiver. The time shift should also be unchanged if the frequency-thickness product $f \cdot d$ is constant, as the Lamb waves will have the same group velocity, c_g. This is confirmed in Fig. 12, where the three respective data sets (solid circles "●" for x_P = 150 mm, f = 100 kHz and d = 1 mm, hollow circles "○" for x_P = 100 mm, f = 100 kHz and d = 1 mm, and hollow triangles "Δ" for x_P = 150 mm, f = 50 kHz and d = 2 mm) all match the simulation for f·d = 0.1 MHz·mm (solid line). The refraction angle β_0 will also be the same for these three datasets, as the phase velocity c_p of the Lamb waves will be identical. Also shown in Fig. 12 are the effects of using a different frequency-thickness product of 0.06 MHz·mm in polycarbonate, with good agreement between simulation (dashed line) and experiment (hollow squares "□"), and the effects of using a different plate material, aluminium, again with good agreement between simulation (dotted line) and experiment (crosses "×").

However, it can be seen in Fig. 4(b) that the initial excitation of the Lamb wave in Plate 2 occurs whilst there is still significant energy remaining in the leaky wave in the flowing fluid. If the transducer separation distance x_P is longer, more of this leaky wave will be absorbed by Plate 2 and converted into a Lamb wave. Hence, with a shorter transducer separation distance x_P, the amplitude of the received leaky wave should then be lower, as was observed experimentally. This also resulted in slightly more scatter in the experimental values obtained with x_P = 100 mm (the hollow circles "○" in Fig. 12).

The time shifts produced by the Lamb waves at 60 kHz and a frequency-thickness product f·d of 0.06 MHz·mm are larger than those at 100 kHz and 0.1 MHz·mm, as expected. The Lamb waves have a phase velocity c_p of 360 m/s at 60 kHz and 440 m/s at 100 kHz, thus the refraction angle β_0 of the leaky Lamb wave is 73.7° at 60 kHz and 52.9° at 100 kHz according to Snell's Law, resulting in a larger geometric shift, x_F. Additionally, the group velocity c_g for Lamb waves at 60 kHz of 610 m/s is lower than the 690 m/s at 100 kHz. Both of these factors affect the time shift, as can be seen in Eq. (11).

For the aluminium plate, a lower frequency of 40 kHz was used to ensure that the refraction angle was not too small due to the faster phase and group velocities of Lamb waves in aluminium. At 40 kHz, c_p was 620 m/s and c_g was 1200 m/s, giving a refraction angle β_0 of 33.5°. The experimental values for aluminium (crosses "×" in Fig. 12) show more scatter, due in part to the shorter path through the fluid flow at the lower refraction angle, and also to the lower signal levels when using Lamb waves in plates with a higher specific acoustic impedance mismatch to air.

However, transmission of ultrasound through the plates depends on a number of factors. When an airborne wave is incident on a plate, some of the energy will be transmitted into the plate and some will be reflected. Mode conversion may also occur. At angles of incidence other than the surface normal ($\alpha_{Tx} > 0°$), the reflection coefficient is known to be a function of the complex wavenumber and has both poles and zeroes at specific real frequencies and incident angles [22,23]. At these angles, the transmission coefficient can approach unity and sufficient airborne energy enters the plate and generates the corresponding Lamb wave mode, which then leaks into the surrounding medium. When the transducers are aligned such that the main planar wave emitted from the transducer aperture is incident at the correct angle, generation and detection of a specific Lamb wave mode is thus optimised. For an incident airborne wave from a finite aperture, the diffracted waves from the transducer edges emit energy over a range of other angles, so both the S_0 and A_0 leaky Lamb wave modes are generated simultaneously but with different intensities, as shown in previous work by the authors [17].

Finally, the flow meter correction factor (the anemometer measured flow velocity divided by the ultrasonically measured flow velocity) was calculated for each experimental scenario, as shown in Fig. 13. It should be noted that the upstream path and the downstream path through the fluid are offset with respect to each other, so that the intersection of the ultrasound with the fluid flow profile is likely to be different in both directions. However, the three configurations that had the same frequency-thickness product f·d of 0.1 MHz·mm and hence the same refraction angle of 52.9° have very similar correction factors (solid circles "●" for x_P = 150 mm, f = 100 kHz and d = 1 mm, hollow circles "○" for x_P = 100 mm, f = 100 kHz and d = 1 mm, and hollow triangles "Δ" for x_P = 150 mm, f = 50 kHz and d = 2 mm in Fig. 13). The two configurations with different refraction angles of 33.5° in the aluminium plate (crosses "×" in Fig. 13) and 73.7° in polycarbonate (hollow squares "□" in Fig. 13) also have different correction factors, suggesting that the angle of interaction with the flow profile was a dominant effect. It should also be noted that as the flow between the plates was not fully developed, this may have contributed to some of the variation in meter correction factors shown in Fig. 13. Different transducer separations, x_P, and refraction angles, β_0, may thus interrogate a slightly different flow profile.

6. Conclusions

In this work, non-contact ultrasonic flow measurement of gas flow using air-coupled leaky Lamb waves was investigated. A simplified two-

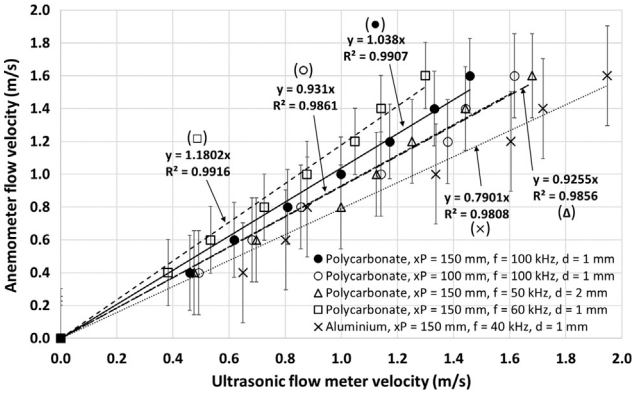

Fig. 13. Experimental flow meter correction factors. (Error bars are 1 standard deviation.)

dimensional approximation of a duct system comprising two thin plates and air flowing between them was modelled and tested experimentally. It was shown that an airborne compression wave emitted from an air-coupled transmitter entered the first plate to excite a Lamb wave. Then leakage of this Lamb wave then propagated through flowing air between the two plates, and entered the other plate to generate a second Lamb wave. Finally, an air-coupled receiver detected the airborne leakage from the second Lamb wave. A simulation model using COMSOL Multiphysics® was implemented successfully to visualize the wave fields and predict the time differences, which were confirmed by an analytical study. The results from experiments examining different testing configurations were in excellent agreement with the proposed theory, and the measured time differences between contrapropagating upstream and downstream paths were used to estimate the flow velocity and determine the meter correction factors. This work has successfully demonstrated the practical feasibility of conducting completely non-contact ultrasonic gas flow measurements in a duct or pipe using air-coupled leaky Lamb waves, and could provide a solution where non-contact applications of flow metering are required in ducts or pipes with thin walls, for example, in air conditioning systems or large diameter gas pipes where direct contact may be difficult.

Acknowledgments

The authors wish to express their gratitude for the financial support for Zichuan Fan from Fundamental Research Funds for the Central Universities (Nos. XDJK2016C150), People's Republic of China, to allow him to conduct research in University College Cork, Ireland while he was a PhD candidate in the School of Automation Science and Electrical Engineering, Beihang University, Beijing, People's Republic of China. Wentao Jiang was supported by Science Foundation Ireland (SFI) Research Frontiers Programme grant number 11/RFP.1/ECE3119 while he was a PhD candidate in University College Cork, Ireland and he is currently a postdoctoral researcher in K.U. Leuven, Belgium.

References

[1] L.C. Lynnworth, Y. Liu, Ultrasonic flowmeters: half-century progress report, 1955–2005, Ultrasonics 44 (2006) e1371–e1378.
[2] R.C. Baker, Flow Measurement Handbook, Cambridge University Press, 2000, pp. 312–356.
[3] J.G. Webster, The Measurement, Instrumentation and Sensors Handbook, CRC Press, Boca Raton, FL, 1999, pp. 28.1–28.11.
[4] M.L. Sanderson, H. Yeung, Guidelines for the use of ultrasonic non-invasive metering techniques, Flow Meas. Instrum. 13 (2002) 125–142.
[5] R.E. Green, Non-Contact Ultrasonic techniques, Ultrasonics 42 (2004) 9–16.
[6] S.P. Kelly, R. Farlow, G. Hayward, Application of through-air ultrasound for rapid NDE scanning in the aerospace industry, IEEE Trans. Ultrason. Ferroelec. Freq. Contr. 43 (1996) 581–591.
[7] K. Tsukada, N. Tsuzuki, H. Kikura, A study of air-coupled ultrasonic flowmeter using beam focusing, Energy Procedia 71 (2015) 352–359.
[8] D.A. Hutchins, W.M.D. Wright, D.W. Schindel, Ultrasonic measurements in polymeric materials using air-coupled capacitance transducers, J. Acoust. Soc. Am. 96 (3) (1994) 2634 1642.
[9] M. Castaings, P. Cawley, The generation, propagation, and detection of Lamb waves in plates using air-coupled ultrasonic transducers, J. Acoust. Soc. Am. 100 (1996) 3070–3077.
[10] L.C. Lynnworth, Ultrasonic Flowmeters *Physical Acoustics*, Academic Press, 1979.
[11] L. Zhou, J.-F. Manceau, F. Bastien, Interaction between gas flow and a Lamb waves based microsensor, Sens. Actuators A 181 (2012) 1–5.
[12] S.G. Joshi, B.D. Zaitsev, I.E. Kuznetsova, Miniature, high efficiency transducers for ultrasonic flow meters. In: Proceedings of the 2004 IEEE Ultrasonics Symposium, vol. 1, 2004, pp.1286–1289.
[13] M.G. Silk, K.F. Bainton, Propagation in metal tubing of ultrasonic wave modes equivalent to Lamb wave, Ultrasonics 17 (1979) 11–19.
[14] G. Liu, J. Qu, Guided circumferential waves in a circular annulus, J. Appl. Mech. 65 (1998) 424–430.
[15] H. Nishino, T. Asano, Y. Taniguchi, K. Yoshida, H. Ogawa, M. Takahashi, Y. Ogura, Precise measurement of pipe wall thickness in noncontact manner using a circumferential lamb wave generated and detected by a pair of air-coupled transducers, Jpn. J. Appl. Phys. 50 (2011) 07HC10.
[16] I.A. Viktorov, Rayleigh and Lamb Waves: Physical Theory and Applications, Plenum Press, New York, 1967.
[17] Z. Fan, W. Jiang, M. Cai, W.M.D. Wright, The effects of air gap reflections during air-coupled leaky lamb wave inspection of thin plates, Ultrasonics 65 (2015) 282–295.
[18] T.H. Gan, D.A. Hutchins, D.R. Billson, D.W. Schindel, High-resolution, air-coupled ultrasonic imaging of thin materials, IEEE Trans. Ultrason. Ferroelec. Freq. Contr. 50 (11) (2003) 1516–1524.
[19] A. Vilpisauskas, R. Kazys, Numerical investigation of air coupled generation of lamb waves in isotropic plates, Elektronika ir Elektrotechnika 20 (2014) 33–36.
[20] J.J. Ditri, K. Rajana, An experimental study of the angular dependence of lamb waves excitation, J. Sound Vib. 204 (1997) 755–768.
[21] COMSOL Multiphysics® User's Guide, Version 4.4, 2013.
[22] D.E. Chimenti, Review of air-coupled ultrasonic materials characterization, Ultrasonics 54 (2014) 1804–1816.
[23] S.I. Rokhlin, D.E. Chimenti, P.B. Nagy, Physical Ultrasonics of Composites, Oxford University Press, USA, 2011 (Chapter 5).